

Electron Cotunneling in a Semiconductor Quantum Dot

S. De Franceschi¹, S. Sasaki², J. M. Elzerman¹, W. G. van der Wiel¹, S. Tarucha^{2,3}, and L. P. Kouwenhoven¹

¹*Department of Applied Physics, DIMES, and ERATO Mesoscopic Correlation Project, Delft University of Technology, PO Box 5046, 2600 GA Delft, The Netherlands*

²*NTT Basic Research Laboratories, Atsugi-shi, Kanagawa 243-0198, Japan*

³*ERATO Mesoscopic Correlation Project, University of Tokyo, Bunkyo-ku, Tokyo 113-0033, Japan*

(October 17, 2018)

We report transport measurements on a semiconductor quantum dot with a small number of confined electrons. In the Coulomb blockade regime, conduction is dominated by cotunneling processes. These can be either elastic or inelastic, depending on whether they leave the dot in its ground state or drive it into an excited state, respectively. We are able to discriminate between these two contributions and show that inelastic events can occur only if the applied bias exceeds the lowest excitation energy. Implications to energy-level spectroscopy are discussed.

PACS numbers: 73.23.Hk, 73.40.Gk, 73.61.Ey

Quantum-dot devices consist of a small electronic island connected by tunnel barriers to source and drain electrodes [1]. Due to on-site Coulomb repulsion, the addition of an electron to the island implies an energy change $U = e^2/C$, where C is the total capacitance of the island. Hence the number of confined electrons is a well-defined integer, N , that can be controlled by varying the voltage on a nearby gate electrode. Transport of electrons through the dot is allowed only at the transition points where the N - and $(N+1)$ -states are both energetically accessible. Otherwise, N is constant and current is strongly suppressed. This is known as Coulomb blockade [1]. At low temperature, however, higher-order tunneling events can become dominant. These are commonly known as *cotunneling* events since they involve the simultaneous tunneling of two or more electrons [2]. Electron cotunneling has received considerable attention over the last decade. Initially it was recognized as a limitation to the accuracy of single-electron devices. More recently, it has acquired a broader relevance, especially since an increasing activity has been focused on quantum dots with a deliberately enhanced tunnel coupling to their leads. These systems allow the investigation of high-order transport processes and many-body phenomena, such as the Kondo effect [3,4]. The latter can be regarded as the result of a coherent superposition of higher-order cotunneling events. Here, we will focus on the lowest order contribution to cotunneling.

Previous experiments were performed with metallic islands [5–7] or large semiconductor dots [8–10], where the energy spectrum is essentially continuous and many levels contribute to cotunneling. Here, we study cotunneling through a small quantum dot where the energy levels are well separated, and where the absolute value of N is pre-

cisely known. A cotunneling event is called inelastic when it leaves the dot in an excited state. Otherwise it is classified as elastic. We identify two regimes: one consisting of elastic processes only, and one including both elastic and inelastic contributions. We note that the transition between these regimes can be sharper than the characteristic life-time broadening of the dot states. In such a case, the onset of inelastic cotunneling can be exploited to measure the energy spectrum of a quantum dot with improved resolution.

The stability diagram of a generic quantum dot can be obtained by plotting the differential conductance (dI/dV_{sd}) as a function of bias, V_{sd} , and gate voltage, V_g . Coulomb blockade occurs within the diamond-shaped regions in Fig. 1a. The diamond size is proportional to the addition energy, defined as $E_{add}(N) \equiv \mu_{dot}(N+1) - \mu_{dot}(N)$, where $\mu_{dot}(N)$ is the electrochemical potential of an N -electron dot. Inside the N -electron diamond, $\mu_{dot}(N) < \mu_L, \mu_R < \mu_{dot}(N+1)$, with μ_L, μ_R the Fermi energies of the leads. The diamond edges correspond to level alignment: $\mu_{dot}(N) = \mu_L$ or μ_R (see angled solid lines). This alignment determines the onset for first-order tunneling via the ground state of the dot, leading to a peak in $dI/dV_{sd}(V_{sd})$. The onset for first-order tunneling via the first excited state occurs at a somewhat higher bias (see dot-dashed lines in Fig. 1a, and the corresponding diagrams in Fig. 1b and 1e). These first-order processes have been exploited as a spectroscopic tool on the discrete energy spectrum of dots [1].

Here, we are interested in second-order tunneling of charge, which becomes more apparent when the tunnel coupling between the dot and the leads is enhanced. We neglect contributions from spin that could give rise to the Kondo effect. Elastic cotunneling is the dominant off-resonance process at low bias. It gives rise to current inside the Coulomb diamond (light-grey region in Fig. 1a). The corresponding two-electron process (Fig. 1c) transfers one electron from the left to the right lead, thereby leaving the dot in the ground state.

For $e|V_{sd}| \geq \Delta(N)$, where $\Delta(N)$ is the lowest on-site excitation energy for a constant N [11], similar two-electron processes can occur which drive the dot into an excited state. For instance, an electron can leave the dot from the ground state to the lowest Fermi sea, while another electron from the highest Fermi sea tunnels into the excited state (see Fig. 1d). Although this type of process is called inelastic [2], the total electron energy is con-

served. The on-site excitation is created at the expense of the energy drop eV_{sd} . To first approximation, the onset of inelastic cotunneling yields a step in $dI/dV_{sd}(V_{sd})$ [12]. This step occurs when $e|V_{sd}| = \Delta(N)$, which is not or only weakly affected by V_g (see also Fig. 1c in Ref. [13]). As a result, inelastic cotunneling turns on along the vertical (dotted) lines in Fig. 1a. At the edge of the Coulomb diamond the condition for the onset of inelastic cotunneling connects to that for the onset of first-order tunneling via an excited state (dot-dashed lines).

Our device has the external shape of a $0.5\text{-}\mu\text{m}$ -high pillar with a $0.6 \times 0.45 \mu\text{m}^2$ rectangular base (inset to Fig. 2). It is fabricated from an undoped AlGaAs(7 nm)/InGaAs(12 nm)/AlGaAs(7 nm) double barrier heterostructure, sandwiched between n-doped GaAs source and drain electrodes [4]. The quantum dot is formed within the InGaAs layer. The lateral confinement potential is close to that of an ellipse [14]. Its strength is tuned by a negative voltage, V_g , applied to a metal gate surrounding the pillar. A dc bias voltage, V_{sd} , applied between source and drain, drives current vertically through the pillar. In addition, we apply a small bias modulation with rms amplitude $V_{ac} = 3 \mu\text{V}$ at 17.7 Hz for lock-in detection. Measurements are carried out in a dilution refrigerator with a base temperature of 15 mK. We find an effective electron temperature $T_e = 25 \pm 5$ mK, due to residual electrical noise.

Figure 2 shows dI/dV_{sd} in grey-scale versus (V_{sd}, V_g) at 15 mK. Diamond-shaped regions of low conductivity (light grey) identify the Coulomb blockade regimes for $N = 1$ to 4. The diamonds are delimited by dark narrow lines ($dI/dV_{sd} \sim e^2/h$) corresponding to the onset of first-order tunneling. For $N = 1$, as well as for $N = 3$, sub-gap transport is dominated by elastic cotunneling with no evidence for inelastic cotunneling. The differential conductance is uniformly low inside the Coulomb diamond. (Slight modulations are seen due to a weak charging effect in the GaAs pillar above the dot [15].) This is different for $N = 2$, where the onset of inelastic cotunneling is clearly observed. As argued before, this onset follows (dotted) lines, nearly parallel to the V_g axis [16]. At the diamond edges they connect to (dot-dashed) lines where first-order tunneling via an excited state sets in. Similar considerations apply to $N = 4$.

The different behavior observed for $N = \text{even}$ and $N = \text{odd}$ stems from the fact that inelastic cotunneling occurs only if $E_{add}(N) > \Delta(N)$, as apparent from Fig. 1a. In the case of non-interacting electrons, $E_{add}(N) = U(N)$ for $N = \text{odd}$ and $E_{add}(N) = U(N) + \Delta(N)$ for $N = \text{even}$, where $U(N)$ is the charging energy for N electrons; energy levels are spin degenerate and consecutively filled with pairs of electrons. This is a reasonable picture if the level spacing exceeds the exchange interaction energy [17]. In our small quantum dot the first three levels are indeed widely spaced as already discussed in Ref. [4]. For low N , $\Delta(N)$ exceeds not only the exchange energy but also $U(N)$. This implies that for $N = \text{odd}$, $\Delta(N)$ lies outside the Coulomb diamond (i.e. $\Delta(N) > E_{add}(N)$)

and thus inelastic cotunneling is not observed. (Note that cotunneling between spin-degenerate states is an elastic process as initial and final state have the same energy.) For $N = \text{even}$, $\Delta(N)$ is always smaller than $E_{add}(N)$ and inelastic cotunneling can be observed.

We now discuss the difference in life-time broadening between first- and higher-order tunneling. At the onset of first-order tunneling a certain level is aligned to one of the Fermi energies. In this case, an electron can escape from the dot, which leads to a finite life-time broadening of the observed resonance by an amount $\hbar\Gamma$. Here, $\Gamma = \Gamma_L + \Gamma_R$, where Γ_L and Γ_R are the tunneling rates through the left and the right barrier, respectively. (Note that these rates are independent of V_{sd} , since our bias window ($\sim\text{meV}$) is much smaller than the height of the AlGaAs tunnel barriers ($\approx 50 \text{ meV}$).

The onset of inelastic cotunneling is also characterized by a width. In the zero-temperature limit, this is determined by the life-time broadening of the excited state. Two types of situations can occur. First, the excited state can be between μ_L and μ_R (see right inset to Fig. 3) so that inelastic cotunneling can be followed by first-order tunneling. Such a decay event leads to a life-time broadening of at least $\hbar\Gamma_R \approx \hbar\Gamma/2$. Second, the ground and excited state are both well below μ_L and μ_R , implying that only higher-order tunneling is allowed (see right inset to Fig. 4). Now, decay from the excited state can only rely on cotunneling. For this higher-order perturbation, the corresponding rate, Γ_{co} , is much smaller than Γ , leading to a reduced life-time broadening. To illustrate these arguments, we select different $dI/dV_{sd} - vs - V_{sd}$ traces and analyse their shape in detail.

Figure 3 shows two traces for $N = 2$, taken at 15 mK for gate voltages at the horizontal lines in the left inset. The dashed trace has several peaks. The two inner ones, at $|V_{sd}| \approx 1.1 \text{ mV}$, correspond to first-order tunneling of the 3rd electron via the 3-electron ground state; i.e. $\mu_{dot}(3) = \mu_L$ or μ_R . The right (left) peak has a full width at half maximum (FWHM) of ≈ 200 (≈ 400) μV . This is somewhat larger than the width, $\hbar\Gamma/e \simeq 150 \mu\text{V}$, measured in the zero-bias limit. Indeed a finite bias allows non-energy-conserving tunneling events leading to additional broadening. The most likely source for energy relaxation is acoustic-phonon emission [18]. The following pair of peaks, at $|V_{sd}| \approx 2 \text{ mV}$, corresponds to the onset of first-order tunneling via the first excited state for $N = 2$ (see Fig. 1b). Because of the larger bias voltage, these peaks are visibly broader than the inner ones. Additional peak structures occur near the edges of the bias window. The origin of these peaks can not be precisely identified.

The solid trace contains structure from both first- and second-order tunneling. The peaks labeled by open squares arise from first-order tunneling at the edges of the Coulomb diamond (see left inset). Steps, labeled by open circles, identify the onset of inelastic cotunneling and correspond to the open circles in the left inset. Their different heights are probably due to a left-right asymmetry

in the tunnel coupling to the leads. Their V_{sd} -position, which is symmetric around zero bias, provides a direct measure of $\Delta(2)$. The width of these steps is $\approx 150 \mu\text{V}$ [19]. Since $\Delta(2) \approx U(2)$, the first excited state lies unavoidably within the bias window when $|V_{sd}| = \Delta(2)/e$ and hence is allowed to decay into the lowest-energy lead (see the right inset to Fig. 3). As argued above, this situation leads to a step-width exceeding $\hbar\Gamma_R/e$, consistent with our finding. Another structure occurs at $V_{sd} \approx 2.6 \text{ mV}$ and is probably due to the onset of inelastic cotunneling via the second excited state for $N = 2$. The corresponding line in the stability diagram is hardly visible due to its vicinity to the diamond edge.

To study inelastic cotunneling when both ground and excited state lie well below the Fermi energies of the leads (Fig. 1d) we need $\Delta(N) \ll E_{add}(N)$. To this aim we move to $N = 6$, since $\Delta(6)$ can be effectively tuned by a magnetic field applied along the vertical axis. We tune the field to 0.35 T, such that $\Delta(6) \approx 0.1 \text{ meV}$, i.e. several times smaller than $E_{add}(6)$. From a previous study we know that the ground state is a spin singlet, and the first excited state is a spin triplet [4]. The $dI/dV_{sd} - vs - V_{sd}$ traces shown in Fig. 4 are taken at two different temperatures, but for the same V_g , at the horizontal line in the left inset. The solid trace (15 mK) shows a broad minimum around $V_{sd} = 0$, where transport is dominated by elastic cotunneling via the ground state (see also the light-grey region in the left inset). The differential conductance increases rapidly at the onset of inelastic cotunneling with a step-width of $\approx 20 \mu\text{V}$, i.e. much smaller $\hbar\Gamma/e$. This reduced width stems from the fact that the excited state can not decay directly into the lower energy lead (see right inset). The corresponding life-time broadening, $\hbar\Gamma_{co}$, can be estimated from the cotunneling current, I_{co} , at $V_{sd} = \Delta(6)/e$. We find $\hbar\Gamma_{co} = \hbar I_{co}/e \approx (\hbar/e) \int_0^{\Delta(6)/e} dI/dV_{sd}(V_{sd}) dV_{sd} \simeq 10 \mu\text{eV}$, consistent with the observed step-width. At $T_e = 25 \text{ mK}$ the thermal broadening of the Fermi distribution functions leads to a step-width of $5.44k_B T_e/e \simeq 12 \mu\text{eV}$ [20]. Hence life-time broadening has been reduced here to the thermal limit.

The cotunneling onset in Fig. 4 shows a peak structure at low temperature (solid trace) in addition to the expected step structure. This is likely due to Kondo correlations, as discussed in Ref. [4]. On increasing temperature to 200 mK these Kondo correlations are suppressed such that only lowest order cotunneling contributes. This recovers the step structure (dashed trace).

We thank Yu. V. Nazarov, M. R. Wegewijs, M. Eto, K. Majjala, and J. E. Mooij for discussions. We acknowledge financial support from the Specially Promoted Research, Grant-in-Aid for Scientific Research, from the Ministry of Education, Science and Culture in Japan, from the Dutch Organisation for Fundamental Research on Matter (FOM), from the NEDO joint research program (NTDP-98), and from the EU via a TMR network.

- [1] L. P. Kouwenhoven, C. M. Marcus, P. L. McEuen, S. Tarucha, R. M. Westervelt, and N. S. Wingreen, in *Mesoscopic Electron Transport*, edited by L.L. Sohn, L. P. Kouwenhoven, and G. Schön, (Kluwer, Series E 345, 1997), p. 105-214.
- [2] D. V. Averin and Yu. V. Nazarov, in *Single Charge Tunneling - Coulomb Blockade Phenomena in Nanostructures*, edited by H. Grabert and M. H. Devoret (Plenum Press and NATO Scientific Affairs Division, New York, 1992), p. 217.
- [3] D. Goldhaber-Gordon *et al.*, Nature **391**, 156, (1998); Cronenwett *et al.*, Science **281**, 540 (1998); Schmid *et al.*, Physica B **256-258**, 182 (1998).
- [4] S. Sasaki *et al.*, Nature **405**, 764 (2000).
- [5] L. J. Geerligs, D. V. Averin, and J. E. Mooij, Phys. Rev. Lett. **65**, 3037 (1990).
- [6] T. M. Eiles *et al.*, Phys. Rev. Lett. **69**, 148 (1992).
- [7] A. E. Hanna, M. T. Tuominen, and M. Tinkham, Phys. Rev. Lett. **68**, 3228 (1992).
- [8] D. C. Glatli *et al.*, Z. Phys. B **85**, 375 (1991).
- [9] C. Pasquier *et al.*, Phys. Rev. Lett. **70**, 69 (1993).
- [10] S. M. Cronenwett *et al.*, Phys. Rev. Lett. **79**, 2312 (1997).
- [11] In our definition $\Delta(N)$ is strictly positive. It reduces to the single-particle level spacing for non-interacting electrons (for instance, in the case of $N = 1$ and $N = 2$, $\Delta(N)$ is the spacing between the first two single-particle levels).
- [12] Y. Funabashi *et al.*, Jpn. J. Appl. Phys. **38**, 388 (1999).
- [13] J. Schmid *et al.*, Phys. Rev. Lett. **84**, 5824 (2000).
- [14] D. G. Austing, *et al.*, Phys. Rev. B **60**, 11514 (1999).
- [15] The top contact is obtained by deposition of Au/Ge and annealing at 400 °C for 30 s. This thermal treatment is gentle enough to prevent the formation of defects near the dot, but does not allow the complete suppression of the native Schottky barrier. The residual barrier leads to electronic confinement and corresponding charging effects in the GaAs pillar.
- [16] V_g affects not only the bottom but also the shape of the confining potential. As a result, the level spacing (and hence $\Delta(N)$) depends weakly on V_g , leading to a non-zero angle between the dotted lines and the V_g axis.
- [17] S. Tarucha *et al.*, Phys. Rev. Lett. **84**, 2485 (2000).
- [18] T. Fujisawa *et al.*, Science **282**, 932 (1998).
- [19] The step-width is estimated by taking the full width at half maximum of the corresponding peak (or dip) in $d^2I/dV_{sd}^2(V_{sd})$.
- [20] E. L. Wolf, *Principles of Electron Tunneling Spectroscopy*, (Oxford, New York, 1985) p. 438.

FIG. 1. (a) Stability diagram in the plane of (V_{sd}, V_g) . Angled lines correspond to *alignment* of a dot-state with the Fermi energy of the leads. In this case, first-order tunneling sets in, or is increased, as illustrated in (b) and (e). In the light-grey area in (a), conduction is due to elastic cotunneling via virtual events as shown in (c). For $eV_{sd} \geq \Delta(N)$, inelastic processes, illustrated in (d), increase the cotunneling current (dark-grey areas). $\Delta(N)$ is the energy spacing between the ground state and the first excited state, which in (b)-(e) are represented by solid and dotted lines, respectively.

FIG. 2. Measured stability diagram of our quantum dot at 15 mK and zero magnetic field. dI/dV_{sd} is plotted in grey scale as a function of (V_{sd}, V_g) . Dotted lines have been superimposed to highlight the onset of inelastic cotunneling. The dot-dashed lines indicate the onset of first-order tunneling via an excited state. Inset: scanning electron micrograph of the device.

FIG. 3. Differential conductance as a function of bias for $V_g = -1.40$ V (solid line) and $V_g = -1.30$ V (dotted line) at 15 mK. These traces are extracted from the stability diagram shown in the left inset. The horizontal lines indicate the corresponding V_g values. The right inset shows the qualitative energy diagram corresponding to the onset of inelastic cotunneling for $N = 2$. The horizontal arrow represents the possibility for an electron in the excited state to decay directly into the right lead by first-order tunneling.

FIG. 4. Differential conductance as a function of bias at $V_g = -0.685$ V. (Note that the bias window is much smaller than in Fig. 3.) The solid (dashed) line is taken at 15 mK (200 mK). Left inset: stability diagram at 15 mK, around the 6-electron Coulomb diamond. The horizontal line is at $V_g = -0.685$ V. Right inset: qualitative energy diagram corresponding to the onset of inelastic cotunneling for $N = 6$.

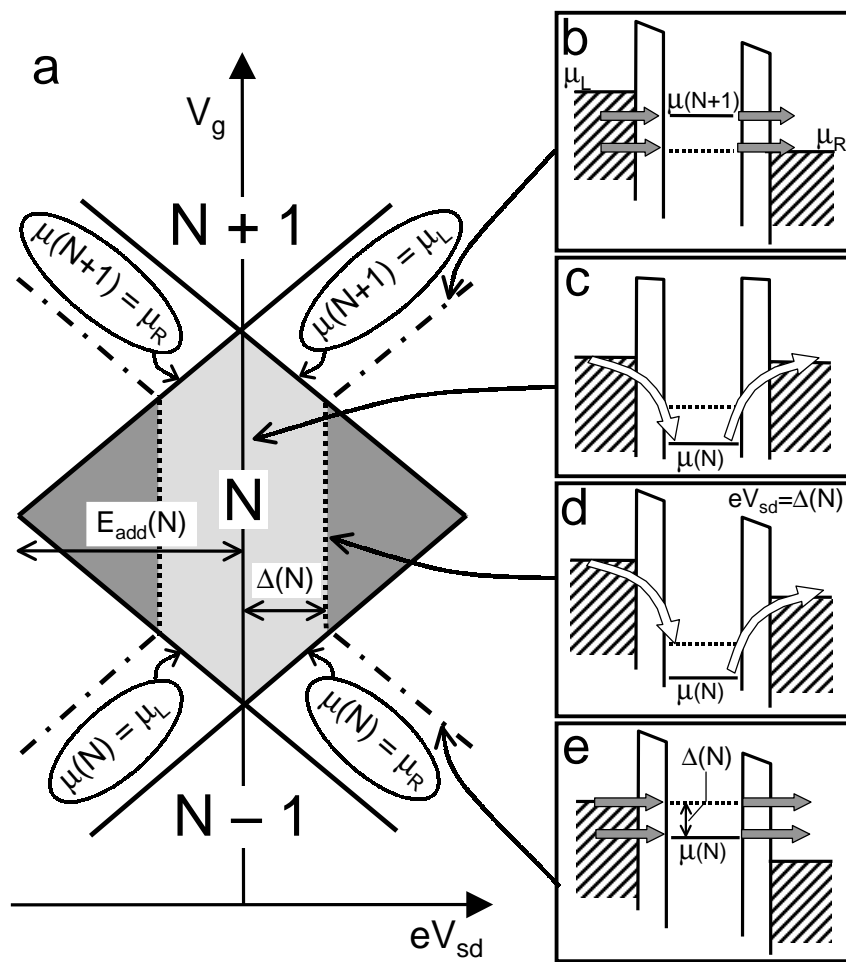


Fig. 1

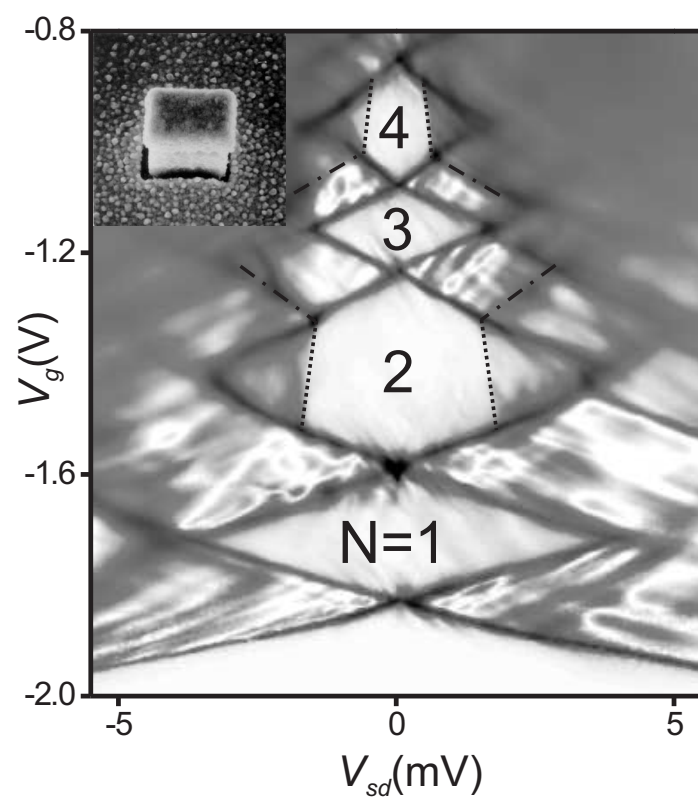


Fig. 2

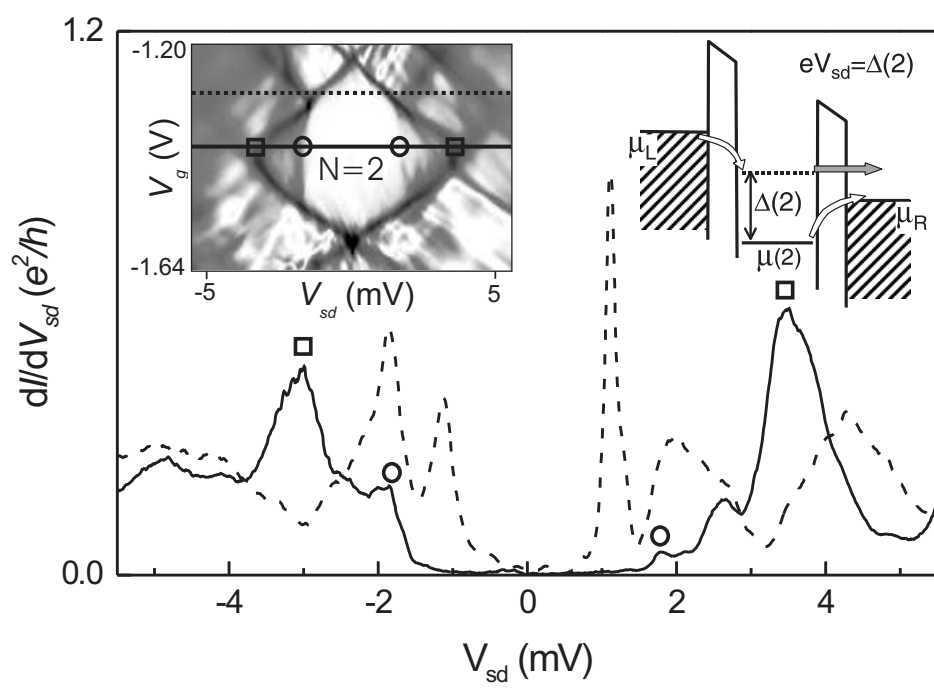


Fig. 3

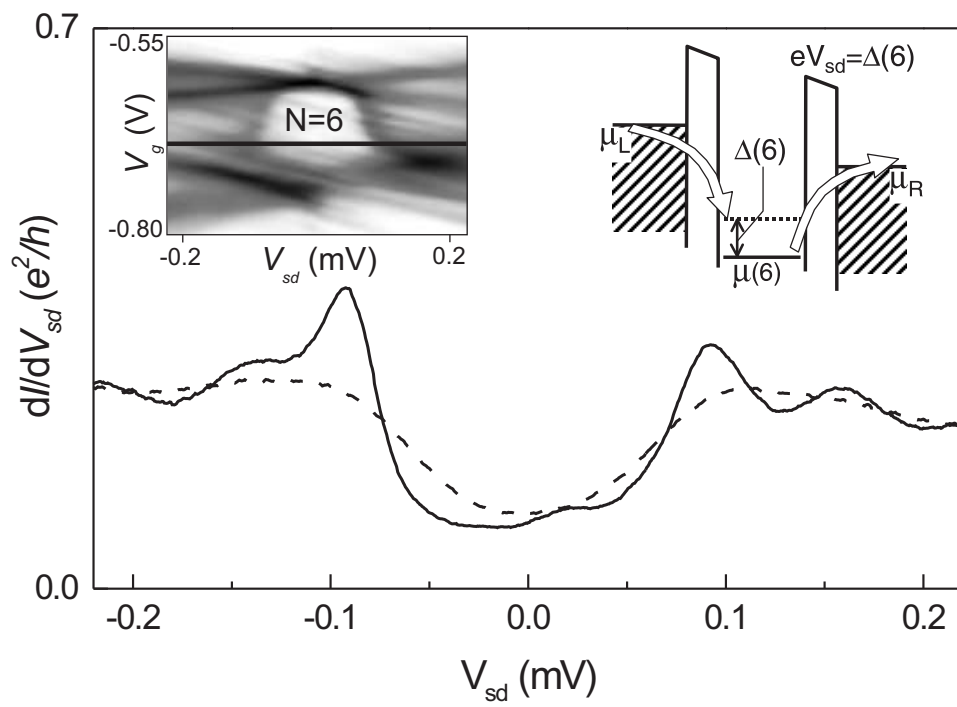


Fig. 4